Healy, F., Cheung, R. C. M., Rezgui, D., Cooper, J. E., Wilson, T., & Castrichini, A. (2021). On the Nonlinear Geometric Behaviour of Flared Folding Wingtips. In *AIAA SCITECH 2022 Forum: Session: Flutter and Limit Cycle Oscillation Problems II* American Institute of Aeronautics and Astronautics Inc. (AIAA). https://doi.org/10.2514/6.2022-0656

Peer reviewed version

University of Bristol - Explore Bristol Research
General rights

On the Nonlinear Geometric Behaviour of Flared Folding Wingtips

Fintan Healy*, Ronald Cheung [†], Djamel Rezgui[‡] and Jonathan Cooper [§]
University of Bristol, Bristol, BS8 1TR, UK

Thomas Wilson[¶] and Andrea Castrichini[‖]
Airbus Operations Ltd, Bristol, BS34 7QQ, UK

Recent studies have considered the use of flared folding wingtips (FFWTs) to enable higher aspect ratios - reducing overall induced drag - whilst reducing gust loading and meeting airport operational requirements. The majority of these analyses have been conducted using linear assumptions despite the presence of large wingtip deformations. The aim of this work is to assess the effect of geometric nonlinearities introduced by an FFWT on the static and dynamic aeroelastic response of a wing. In this paper, a geometrically exact expression was formulated to describe the change in both the local Angle of Attack (AoA) and sideslip angle across all fold angles. This expression highlighted that the aerodynamic stiffness of an FFWT, and therefore quantities such as the linear flutter speed, are a function of the fold angle and therefore, the attitude of the wing. This effect was then verified using both: a wind tunnel model of a flexible semi-span wing incorporating an Flared Folding Wingtip (FFWT), and a new numerical modelling technique, utilising MSC Nastran, which linearised the model about the equilibrium position of the wingtip. The results of these experiments show that the geometric nonlinearities introduced due to the large deformations of FFWTs can significantly affect the dynamics of the system, with flutter speeds varying by over 25%, simply by changing the root angle of attack of the model. Furthermore, good agreement was found between the experimental results and numerical predictions.

I. Nomenclature

C_l	=	lift coefficient
C_l^*	=	wingtip corrected lift coefficient
c	=	wing chord
D	=	drag force
f	=	frequency
g	=	acceleration due to gravity
$\vec{\mathbf{H}}_n^m$	=	the transformation matrix from the 'n'th to the 'm'th frame of reference
K	=	Stiffness
k	=	lag or delay in the auto-correlation
$\bar{L}$	=	lift force per unit span
L	=	Lift force
l_i	=	moment arm between the hinge line and the 'i'th mass on the wingtip
M	=	hinge moment
m_i	=	'i'th wingtip mass
R_n	=	3D rotation matrix about the 'n'th axis
$\hat{r}$	=	auto-correlation

*PhD Student, Department of Aerospace Engineering.
[†]Research Associate, Department of Aerospace Engineering.
[‡]Senior Lecturer, Department of Aerospace Engineering MAIAA.
[§]Airbus RAEng Sir George White Professor of Aerospace Engineering, Department of Aerospace Engineering, FAIAA
[¶]Head of Technical Capability for Aircraft Loads, Flight Physics
[‖]Loads and Aeroelastics Engineer, Flight Physics

s	=	generic time signal
u	=	wind speed
$\vec{\mathbf{v}}$	=	velocity vector
w	=	downwash
α	=	angle of attack
β	=	aircraft sideslip angle
θ	=	fold angle
Λ	=	flare angle
ρ	=	density
γ	=	sweep angle
Γ	=	local dihedral angle
$\vec{\phi}$	=	mode shape

Subscripts

b	=	in the body frame of reference
c	=	at the coast angle
h	=	at the tip of the inner wing (the hinge)
t	=	in the wingtip frame of reference
w	=	in the wind frame of reference
g	=	due to gravity

II. Introduction

To drive the development of the next generation of green aircraft, recent schemes such as the ICAO *CORSIA* scheme aim to place a cost on emissions [1], incentivising the industry to improve overall aircraft efficiency through the use of radical design solutions. Many such solutions have aimed to improve efficiency by increasing the wingspan and therefore aspect ratio of future aircraft. A recent conceptual design study by Calderon et al. [2] showed that, even when weight is considered, the optimal wingspan is much larger than current designs. However, increasing the span of the next generation of aircraft also increases their operational cost, with airport fees calculated according to span [3] and current infrastructure at many airports - such as gate, runway and taxiway separation - only capable of servicing aircraft up to a specific span [4, 5].

Therefore, Folding Wingtip (FWT) devices, in which the span of the aircraft can be shortened on the ground by folding the wingtips up, have gained popularity. This type of device is not new, with military aircraft using the concept to save space on aircraft carriers since as early as the first world war [6]. The most notable recent example is the Boeing 777X, which first flew in 2020, allowing the aircraft to fit into the same 65m gate as its predecessor, whilst also being able to increase its wingspan in flight by 7 metres [7]. Whilst the wingtips of the 777X can only be operated on the ground, the inclusion of such a mechanism raised the question as to whether folding wingtips can be utilised in-flight for aerodynamic or structural benefits. One such solution is the FFWT [8–16]. As illustrated in Fig. 1, this device consists of a FWT in which the hinge line is rotated so that it is no longer parallel with the oncoming flow, with the magnitude of this rotation being defined as the flare angle (Λ). In this configuration an increase in the fold angle (θ) produces a decrease in the local AoA of the wingtip, and vice versa. Castrichini et al. [11] described this relationship as

$$\Delta\alpha = -\arctan\left(\sin\Lambda\tan\theta\right) \tag{1}$$

Therefore, when an FFWT is free to rotate, the fold angle tends to an equilibrium position, defined as the coast angle, at which the aerodynamic and gravitational moments about the hinge balance, and the system is statically stable.

Utilising the fact that only shear forces are transmitted through a hinge with both zero stiffness and damping, initial experimental [10, 15] and numerical [9, 11, 17] research on this concept was focused on its use as a passive gust alleviation device, with results showing wing loading can be significantly reduced during manoeuvres and gust encounters. More recent numerical sizing analysis [16] has shown that the inclusion of FFWTs on a typical transonic aircraft could reduce the required primary wing mass by up to 30%. Much of this numerical research was limited to linear analysis, by assuming small displacements about a fold angle of zero degrees - either implicitly by use of linear finite element analysis, or explicitly using Eq. (1), which is derived by assuming small displacements about a fold angle

of zero degrees [11]. However, coast angles with a magnitude over 20 degrees have been reported in the majority of studies, including experimental test flights of an Unmanned Aerial Vehicle (UAV) incorporating FFWTs [18] and a wind tunnel experiment utilising FFWTs to enhance the roll authority of an aircraft [19]. Such large deformations are analogous to those seen in the modelling of highly flexible wings [20], and can introduce geometric and aerodynamic nonlinearities that significantly affect the overall system dynamics.

A few authors have begun to explore the effects of including such nonlinearities on the response of FFWTs. Wilson et al. [21] created a geometrically nonlinear structural model by discretising a cantilever wing as a set of rigid rods connected by bending and torsional springs. This model was used to explore if FFWTs could exhibit limit cycle oscillations. However, the aerodynamics of this model were underpinned by evaluating the local AoA of an FFWT using Eq. (1), which was derived using small angle approximations. An extension to Eq. (1) was derived by Cheung et al. [15] to calculate a more accurate local AoA for an FFWT across a wider range of fold angles, which was then used to better predict the coast angle of an FFWT, with good correlation to experimental data. However, this formulation did not account for other geometric nonlinearities such as the change in the sweep angle of the wingtip with fold angle (which can be visually seen in Fig. 1), or the local dihedral angle at the tip of the inner wing - which can change with the deformation of the inner wing.

Additionally, at higher fold angles the aerodynamic influence of a FWT on the inner wing, and vice versa, can vary due to the significant changes in the geometry of the wing (varying spanwise lift distribution). Conti et al. [22] developed the Equations of Motion (EoM) for a representative civil aircraft, with aerodynamic and structural corrections to account for the geometric nonlinearity due to FFWT displacements. The aerodynamics were modelled using the doublet lattice method, with the boundary condition on the wingtip panels being defined using a coordinate transformation between a body reference frame and a reference frame centred about a "deformed" wingtip. Additionally, the change in aerodynamic "influence" between the wingtip and inner wing was accounted for by augmenting the respective aerodynamic influence coefficients using a cosine relationship. This formulation was used to show that accounting for geometric nonlinearities significantly affects the coast angle of FFWTs.

The current studies in the field have primarily focused on the nonlinear static aeroelasticity of FFWTs. However, variations in the dynamic aeroelastic response may equally be of importance. Arguably the most important dynamic aeroelastic phenomenon is flutter, where over some critical speed, known as the linear flutter speed, an initial disturbance will cause an unstable oscillation to grow exponentially [23], unless it is bounded by some form of nonlinearity . The onset of flutter would generally lead to the catastrophic loss of an aircraft. Therefore, aircraft are designed to ensure that the achievable flight envelope is free from aeroelastic instabilities such as flutter.

One potential drawback of FFWTs is the creation of an additional mode of vibration with a natural frequency which, in analysis linearised about a fold angle of zero, grows linearly with velocity from zero [11]. As this mode approaches the first bending mode the system can become unstable, significantly reducing the linear flutter speed of an aircraft. Currently, no studies have addressed how the dynamic response and stability of a flexible wing including FFWTs varies due to geometric nonlinearities. Therefore, in this paper a flexible wind tunnel model is used to demonstrate how large nonlinear geometric deformations of a wing incorporating FFWTs can affect the dynamic response and in particular the flutter speed of the system. The experimental data is complemented with the formulation of a new numerical modelling
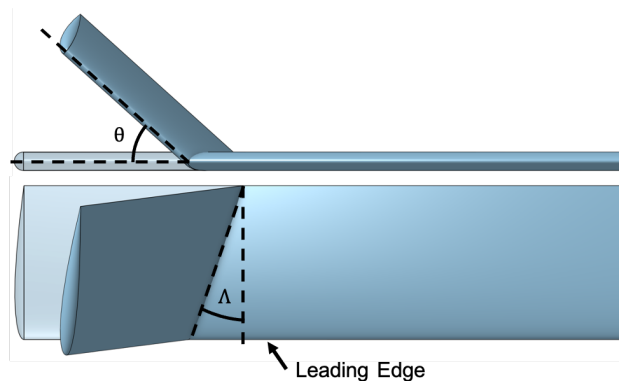

Fig. 1   Representation of a flared folding wingtip device, with a flare angle (Λ) of 20 degrees, at 0 and 45 degrees fold angle (θ)

technique which linearises a model, developed in MSC Nastran [24], about the deformed state of a wing. Such a model captures the geometric nonlinearities caused by the large deflections of a wingtip and allows for the accurate prediction of flutter speeds, with a good correlation seen between the numerical and experimental results.

III. Geometrically Exact Representation of the Effective Angle of Attack

The fundamental mechanism of an FFWT is how the local AoA of the wingtip changes as a function of the fold angle, for a given flare angle. Castrichini et al. [11] described this effect using Eq. (1), which will be referred to as the Small Angles Model (SAM). The formulation of the SAM assumes small deformations about a fold angle of zero degrees, and is therefore only applicable for small deformations. In this section, a new formulation is derived to accurately account for all the nonlinear geometric effects associated with large fold angles. Its derivation differs to those presented in [12, 15] by considering both the change in sweep of the wingtip with fold angle and the effect of the inner wing twist. It is however similar to that presented by Conti et al. [22], albeit the resulting equation was only used to define the boundary conditions on the wingtip panels within there aerodynamic model, whereas here it will be used to understand some of the fundamental mechanisms driving the nonlinear dynamics of FFWTs.

To develop such a model a set of rotation matrices were utilised to transform an aircraft's velocity vector into a reference frame centred about the FFWT, as illustrated in Fig. 2. To facilitate this goal, the standard notation of a body and wind reference frame [17] are used to represent the orientation of the aircraft and its direction of motion respectively. In the wind reference frame the x axis points along the direction of motion of the aircraft and the z axis against the 'line of action' of the lift force. In the body frame of reference the x axis points forwards along the fuselage, and the y axis is perpendicular to the plane of symmetry of an aircraft and points out towards the starboard wingtip. In the FFWT frame of reference, the y axis points along the leading edge of the FFWT (towards the tip of the starboard wingtip), and the z axis is perpendicular to the plane defined by the y axis and the chordline of the FFWT (pointing vertically down at a fold angle of zero degrees). In the wind reference frame the velocity vector has the form

$$\vec{\mathbf{v}}_w = \begin{bmatrix} u & 0 & 0 \end{bmatrix}^T \tag{2}$$

where u is the wind speed. The transformation matrix from the wind to body reference frame is defined as

$$\mathbf{H}_w^b = \mathbf{R}_z(\beta)\mathbf{R}_y(\alpha) \tag{3}$$

where $\mathbf{R}_n(m)$ is the 3D rotation matrix which describes an anti-clockwise rotation about the nth axis by m radians, α is the AoA of the aircraft, and β is the aircraft sideslip angle. The transformation matrix from the body to the FFWT
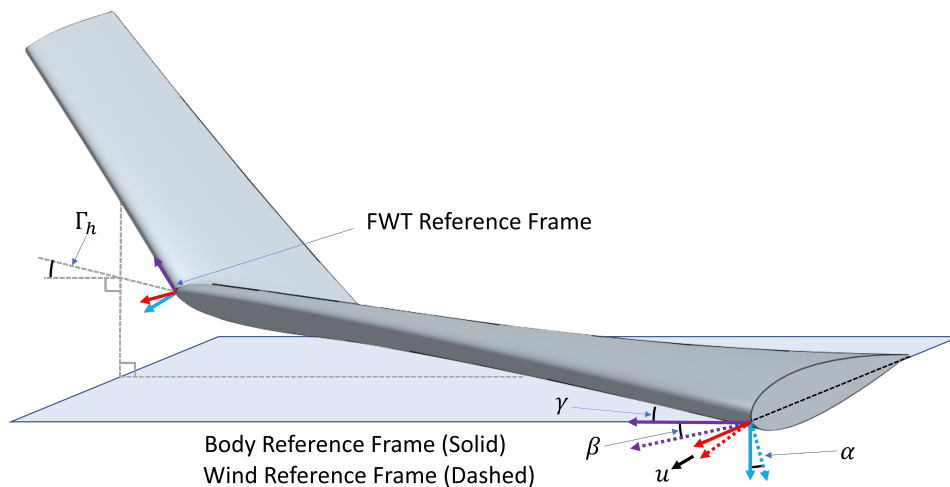

Fig. 2   A visual representation of the body, wing and FWT reference frames used in the geometrically exact formulation

4

reference frame is defined as

$$\mathbf{H}_b^t = \mathbf{R}_x(\Gamma_h)\mathbf{R}_z(\Lambda)\mathbf{R}_x(\theta)\mathbf{R}_z(\gamma - \Lambda) \tag{4}$$

where γ is the geometric sweep of the wingtip - with a positive angle corresponding to an aft-swept configuration, and Γ_h is the local dihedral angle at the hinge (the tip of the inner wing). Considering Eq. (4) and reading from right to left, the first two rotations align the x axis with the hinge line, the third rotation ensures the y axis lies in the XY plane of the wingtip, and the final rotation aligns the y axis with the leading edge of the wingtip. Therefore, the following operation transforms an aircraft's velocity vector into the FFWT reference frame, such that

$$\vec{\mathbf{v}}_t = \begin{bmatrix} v_{t1} & v_{t2} & v_{t3} \end{bmatrix}^T = \left(\mathbf{H}_w^b \mathbf{H}_b^t\right)^T \vec{\mathbf{v}}_w = \mathbf{H}_t^w \vec{\mathbf{v}}_w \tag{5}$$

which is the local velocity vector of an FFWT using the Geometrically Exact Model (GEM). It is valid for a rigid FFWT at all values of flare angle, fold angle, root AoA, sideslip, sweep and local dihedral angle. Two key parameters can be calculated from Eq. (5), the local AoA and local sweep angle of the FFWT, which are defined respectively as

$$\alpha_t = \arctan\frac{v_{t2}}{v_{t0}} \tag{6}$$

$$\gamma_t = \arctan\frac{v_{t1}}{v_{t0}} \tag{7}$$

Exploration of these parameters highlights three primary nonlinear mechanisms acting on an FFWT:

Flare-Twist Effect - As has already been described in literature [11], there is a geometric coupling between the local AoA of an FFWT and the fold angle. This change is driven by the flare angle and can be considered as a uniform twist of the FFWT. Figure 3 shows that for a non-zero flare angle, as the fold angle increases the local AoA decreases. Importantly, the GEM predicts a maximum local AoA, the magnitude of which is approximately the flare angle. Whereas Fig. 3 shows that the SAM over predicts the local AoA at higher fold angles, when compared to the . With noticeable differences between the two models occurring from around 30 degrees fold angle. The peak of the GEM does not always occur at 90 degrees fold angle, with increasing flare angle increasing both the relative magnitude, and the fold angle at which the peak occurs.

Flare-Sweep Effect - There is a geometric coupling between the local sweep angle of an FFWT and its fold angle. As shown in Fig. 4, compared to the zero-fold-angle, the local sweep angle always decreases with fold angle (e.g. becomes more forward swept), and the maximum theoretical magnitude of this variation is twice the flare angle. For a straight or forward swept wing this means the absolute sweep angle always increases with fold angle, reducing the local chord-wise velocity. In the case of an aft-swept wing, such as on a typical transonic aircraft, the absolute sweep
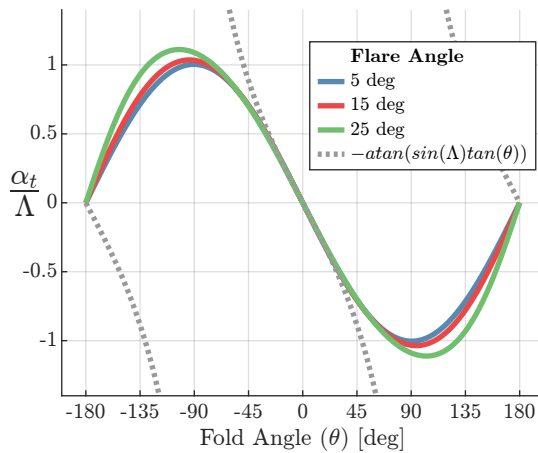

Fig. 3 The variation in the local AoA of an FFWT as a function of the fold angle, at zero root AoA, normalised by the flare angle
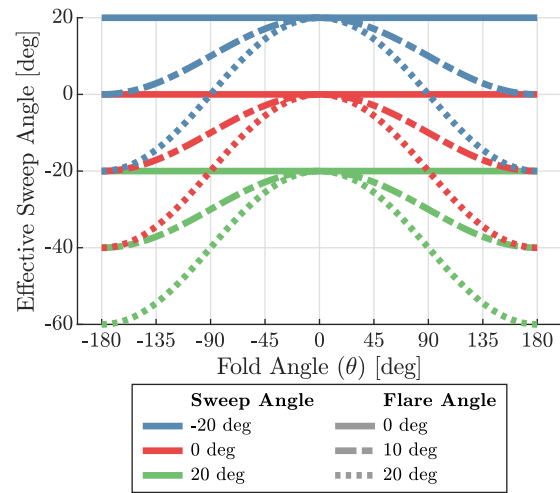
Fig. 4 The variation in the effective sweep angle of an FFWT as a function of fold, flare, and geometric sweep angle, at zero root AoA

angle initially reduces with fold angle - increasing the chord-wise velocity - until a local sweep angle of zero degrees is reached, at which point the chord-wise velocity begins to reduce. As these changes are proportional to the cosine of the local sweep angle, at lower fold angles this effect is most noticeable on a pre-swept wing. It is also important to not that this effect is not captured in models linearised about zero-fold-angle, such at the SAM.

Fold-AoA Effect - For a non-zero root AoA, at all flare angles (including zero degrees), both the local AoA and sweep angle of an FFWT vary as a function of the fold angle. As illustrated in Fig. 5, these variations can be well approximated by a trigonometric relationship, and have a magnitude proportional to the root AoA. Therefore, in configurations or flight conditions in which the root AoA is a significant proportion of the flare angle, this effect will have a significant impact on the response of an FFWT.

In most cases the change in the local AoA and local sweep angle of an FFWT is due to a combination of the *flare-twist*, *flare-sweep* and *fold-AoA* effects. Figure 6 shows this combined effect for a straight wing at varying flare and root AoAs. From Fig. 6 it can be seen that for a non-zero root AoA, the response of an FFWT is asymmetric about the zero fold angle, with the point of maximum and minimum local AoA not occurring at ±90 degrees fold angle. This asymmetry is driven by the combination of the *flare-twist* and *fold-AoA* effects. In configurations in which the flare angle is comparable to the maximum root , a significant proportion of the change in local AoA of the wingtip is due to the fold-AoA effect. Therefore, the response of GEM at low flare angles will vary more with root AoA, as shown in Fig.6. Likewise, at larger flare angles, the *flare-twist* effect dominates and there is significantly less variation in the in the local AoA of the wingtip with root AoA.

In previous studies, such as ones based around the SAM, only the variation in the local AoA has been considered. However, the change in local sweep angle will also affect the aerodynamic forces acting upon an FFWT. As a first approximation, by assuming the streamwise component of the local velocity vector does not affect the aerodynamics [25], the lift per unit span ($\tilde{L}$) of an FFWT can be approximated as
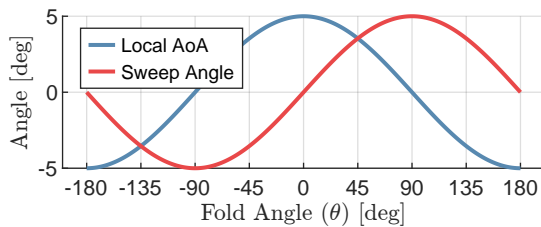

Fig. 5 The variation in the local AoA and effective sweep angle of an FFWT as a function of fold angle, at zero flare angle and a root AoA of 5 degrees
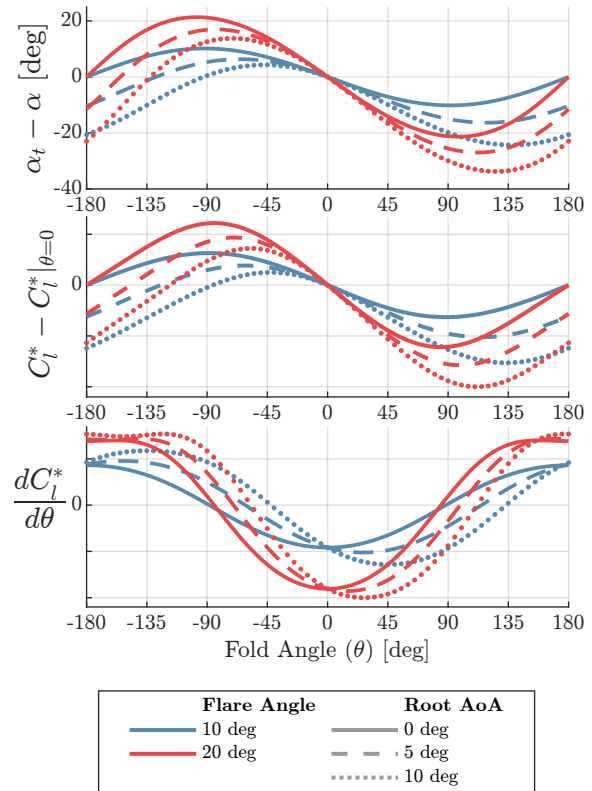

Fig. 6 The variation in local AoA, the FFWT coefficient, and its derivative, with respect to the fold angle, for an unswept wing across a range of flare and root AoAs

6

$$\tilde{L}_t \approx \frac{1}{2}\rho(v_{t0}^2 + v_{t1}^2)c\,C_1(\alpha_t) = \frac{1}{2}\rho\|\vec{v}_t\|^2 c C_l^* \tag{8}$$

$$C_l^* = \frac{v_{t0}^2 + v_{t1}^2}{\|\vec{v}_t\|^2}\,C_1(\alpha_t) \tag{9}$$

where C_l is the local lift coefficient of the unswept wing section, c is the local chord, and C_l^* represents the local lift coefficient corrected for the change in local AoA and sweep angle, with fold angle. An example variation in C_l^* and its derivative with respect to the fold angle, are shown in Fig. 6. This figure shows that for a straight wing, the peak aerodynamic force occurs at a lower fold angle than the peak local AoA, with this effect becoming more pronounced at higher flare angles (due to the increased influence of the *flare-sweep* effect). It is envisaged this variation in C_l^* would be larger for configurations with a non-zero geometric sweep angle, and therefore, the reduction in chord wise velocity with fold angle would be an important mechanism on a typical commercial jet aircraft.

The derivative of C_l^* with respect to the fold angle is analogous to the aerodynamic stiffness of the FFWT, it indicates the change in the aerodynamic forces acting on an FFWT due to a small perturbation of the fold angle, with a negative value corresponding to a stable system. Figure 6 shows there is a large variation in the aerodynamic stiffness of an FFWT with fold angle. Moreover, the aerodynamic stiffness is a function of root AoA, with an increasing root AoA increasing both the magnitude and location of the peak aerodynamic stiffness.

When only aerodynamic forces are considered, changing the root AoA also changes the range of fold angles over which a wingtip is stable. As shown in Fig. 6, for a flare angle of 10 degrees, the stability region varies from $\pm 90\,\mathrm{deg}$ at a root AoA of zero, to between -45 and $+135$ degrees at a root AoA of 10 degrees. As you increase the flare angle this variation in the stability region reduces, due to the decreased significance of the *fold-AoA* effect. Importantly, at a fold angle of zero degrees, the aerodynamic stiffness of an FFWT is independent of the root AoA, explaining why the variation in aerodynamic stiffness were not observed in models linearised about this position.

One of the key design criteria identified in the current research on FFWTs is the frequency of the FWT mode. Castrichini et al. [11] provide a first order approximation of

$$f \propto \frac{1}{2\pi}\sqrt{\frac{K_{aero}(1 - \zeta_n^2)}{I_{\theta wt}}} \tag{10}$$

where K_{aero}, ζ_n and $I_{\theta wt}$ are respectively the aerodynamic stiffness, modal damping and moment of inertia of an FFWT. This mode typically starts from a low frequency and then increases linearly with speed until it interacts with another mode - typically the first bending mode - leading to significantly reduced flutter speeds when compared to an aircraft with a fixed wingtip [11]. In previous analysis the aerodynamic stiffness was assumed to only be a function of velocity and the flare angle, meaning the flare angle and the moment of inertia of an FFWT were considered the only parameters which could be varied to control this frequency, with significant variations in the flutter speed being achieved by altering these parameters.

However, as shown in Fig. 6, the aerodynamic stiffness of an FFWT is in fact a function of both the fold angle and the root AoA. This observation leads to the conclusion that the dynamic response of a wing incorporating FFWTs, and hence parameters such as the linear flutter speed, vary as a function of fold angle and an aircraft's attitude. Additionally, as the peak aerodynamic stiffness of an FFWT occurs at a non-zero fold angle, the frequency of the wingtip mode may be larger than that predicted using models linearised about the zero-fold-angle. This effect means flutter speeds lower than that predicted with traditional techniques could exist in systems incorporating FFWTs. As such, the experimental and numerical models developed within the rest of this paper aim to capture both this effect, and more generally, the aeroelastic response of an FFWT at large fold angles.

IV. Description of Experimental Setup

This work considers a series of tests conducted using the same highly flexible semi-span model as detailed by Cheung et al. [15], with the addition of a new wingtip configuration. The model has a semi-span of $1.345m$ and a constant chord length of $15cm$. The new wingtip configuration has a constant NACA0015 cross-sectional profile, a flare angle of 10 degrees, and a hinge line that intersects the quarter chord line at a distance of $1m$ from the root of the wing. When compared to the previous model this wingtip has a *clean* aerodynamic surface, reducing secondary 3D

effects. As shown in Fig. 7, the model is equipped with an RLS RM08 rotary encoder* in the hinge, a wheatstone bridge measuring the bending moment at the root, and 6 accelerometers distributed across the wing to enable the measurement of the modal shapes and frequencies. All of the instrumentation was connected to a selection of National Instruments PXI cards[†] hosted within a National Instruments PXIe-1082 chassis, with the Matlab Data Acquisition API [26] being utilised to collect the data.

A. Methodology

Testing was carried out in the 7ft by 5ft low-speed closed-return wind tunnel at the University of Bristol. The model, which is shown in Fig. 8, was tested across a range of wind speeds between 14 and $26ms^{-1\ddagger}$, and four root AoA (2.5, 5, 7.5 and 10 degrees). At each test point two methods were used to excite the model. Firstly, the wind tunnel is equipped with a dual-vane vertical gust generator [27], this was used to excite the model with a quasi-random continuous turbulence sequence, generated using the Von Kármán velocity spectra [28]. By using broadband turbulence, this method aimed to excite all modes of the wing structure. Secondly, the model was excited by pulling the wing down, using a string that was attached just inboard of the hinge, on the quarter chord line. The string was then quickly released, producing a step response. This method aimed to only excite the wings bending and FFWT pendulum modes, which are shown in section VI.B to be the primary modes contributing to the flutter mechanism of the wing. Additionally the "Step Response" method was conducted a few months after the "Random Gust Excitation" method, hence with growing confidence in the response of the model, and the ability to pull the string taut to damp out instabilities, speeds closer to the flutter boundary were tested.

For both excitation methods, modal analysis was conducted to estimate the frequency and damping of the first two modes. Due to the presence of large damping ratios and close modal frequencies in certain test conditions, a time-domain method was selected for this analysis [29], in particular the Eigensystem Realization Algorithm (ERA) [30] was utilised. This method requires an impulse response as an input. Farrar and James III [31] demonstrated that the auto-correlation of an accelerometer output represents the impulse response of the original system. For a real valued signal, $s(t)$, the auto-correlation is defined as

$$\hat{r}(k) = \frac{1}{N} \sum_{n=0}^{N-1} s(n)s(n+k) \tag{11}$$

which represents the correlation between the signal and a delayed copy of itself. Where the delay, k, can be varied to

Fig. 7   An overview of the flexible semi-span model

Fig. 8   The wind tunnel model coasting at a stable equilibrium position

8

generate a new signal. Figure 9 shows example time histories, as well as calculated auto-correlations, for each method of excitation. In particular, note how in Fig. 9a the auto-correlation has 'extracted' a step response from a near random signal.
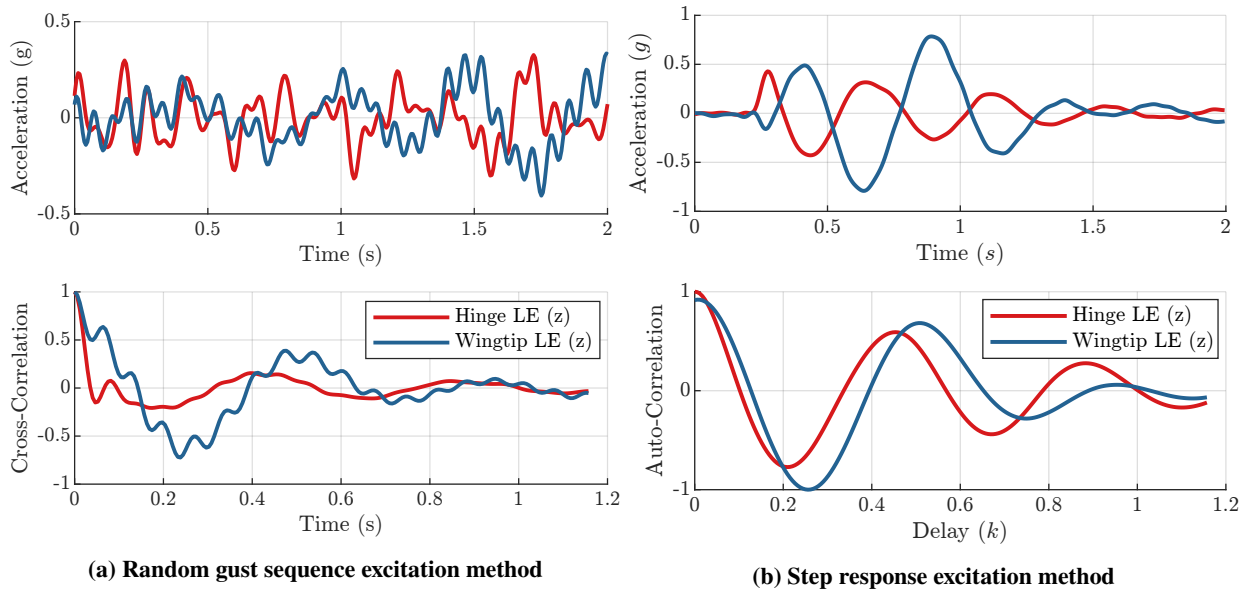

(a) **Random gust sequence excitation method**

(b) **Step response excitation method**

Fig. 9   Example time histories and auto-correlation functions for two accelerometers when the wing was excited using two excitation methods

V. Numerical Modelling

The software package MSC Nastran [24] has been used extensively to model aeroelastic systems in both industrial and academic settings. In particular, much of the literature on FFWTs has previously utilised this tool [10, 11, 14, 16, 22]. Therefore, this section presents a new methodology to model the geometric nonlinearities associated with the large deformations of FFWTs within MSC Nastran.

A baseline linear model (which will be referred to as the baseline model) was first developed to represent the experimental setup. As shown in Fig. 10, the model consists of multiple *CBEAM* elements distributed along the quarter chord to represent the internal stiffness of the wing, as well as a set of distributed concentrated masses to represent the rest of the structure. The hinge is modelled as two coincident nodes connected via an *RJOINT* element with a coordinate system aligned to the hinge axis. The hinge could also be locked by applying at constraint between these two nodes, and in this configuration the distribution of both *CBEAM* elements and concentrated masses was tuned to match the modal frequencies of the experimental model below 15 Hz.

The aerodynamic forces acting on the wingtip are modelled using an implementation of the Doublet Lattice Method (DLM)[32–34], with linear deformations of the underlying structural model being accounted for in the final estimation of aerodynamic loads [35]. As shown in Fig. 10, a total of 1200 aerodynamic panels were used to model the wing, with these panels being split into two sections to model both the inner wing and wingtip separately, with both sections containing 600 panels. This level of discretization was driven by a mesh convergence study focusing on the coast angle of the wingtip in multiple configurations. In MSC Nastran all aerodynamic panels must be coplaner with the streamwise axis, and the sides of each panel must also be parallel with the x axis. Therefore the two sections were split by the chord-line that intersects the hinge line at the semi-chord, as shown in Fig. 10.

Finally, the influence of the tunnel walls was considered by modelling them as additional aerodynamic panels that stretch far into the upstream and downstream directions, with the flow tangency condition on each panel ensuring no flow passes 'through' the walls.

A. The LACA Model

One of the primary limitations of MSC Nastran is in the implementation of the aeroelastic analysis modules, which are limited to linear structural analysis. In the static aeroelastic module (*SOL144*) the aerodynamic loads are modelled using an implementation of the DLM[32–34], with linear deformations of the underlying structural model being accounted for in the final estimation of aerodynamic loads [35]. This analysis is built on the assumption of small-displacements, which is not valid for both highly-flexible wings or wings incorporating FFWTs. To augment *SOL144*, or other aerodynamic solvers, with nonlinear geometric deformations, previous researchers have coupled aerodynamic solvers with the nonlinear structural analysis module (*SOL106*) within MSC Nastran [20, 36, 37]. In general these methods use the following process; the aerodynamic solver is run, ignoring structural deformations, to get an estimate of the aerodynamics loads. These loads are then applied to the Nastran model as constant 'fixed point loads' and a *SOL106* analysis is conducted to estimate the nonlinear geometric deformations. The aerodynamic mesh is then updated to match the deformed shape, and the process repeated until the solution converges.

As is explained in the rest of this paragraph, this type of analysis is not feasible when considering the deformation of an FFWT. In terms of load alleviation, Castrichini et al. [11] concluded that the best configuration for an FFWT is to have a hinge with zero structural stiffness, which is the configuration used throughout this paper. In this configuration the fold angle about which the model is in equilibrium is solely due to how the aerodynamic forces vary with fold angle, rather than a balance of aerodynamic forces with 'internal' strain. Therefore, if a constant aerodynamic force was applied to the wingtip, as required in the aforementioned methodology, an infinite fold angle would be predicted. However, a key feature of these methodologies is to alter the aerodynamic mesh to closely match the deformed shape of the wing, which will be replicated in this paper. This approach ensures that the aerodynamic loads follow the deformed shape of the lifting surface, instead of always being aligned relative to the undeformed position, as in the linear solutions.

At a given flight velocity - below the flutter speed - an FFWT stabilises at an equilibrium position called the *coast angle*. The process outlined below aims to ensure the numerical model is Linearised About the Coast Angle (LACA) by altering the structural and aerodynamic meshes of the baseline model to closely match the flight-shape of the deformed wingtip at each test condition. In this paper the emphasis is on capturing the effect of large deformations of the FFWT, therefore the deformation of the inner wing will be assumed to be linear. Due to the flexibility of the experimental model this assumption may reduce the accuracy of the simulations, however this effect was deemed to be second order when compared to the effect of the FFWT, as presented in the rest of this paper.

An example of the 'altered' structural and aerodynamic models can be seen in Fig. 10. To deform the structural

model, all nodes on the wing are rotated by the root AoA, and all nodes on the wingtip are rotated about the hinge line by the coast angle. To deform the aerodynamic mesh, the panels on the wingtip are rotated about the chord-line the intersects the hinge-line, by the fold angle. Note, as the aerodynamic panels must be parallel with the flow, this rotation does not occur about the hinge-line, as such the change in the local AoA and sweep angle is not accounted for in this rotation.

To account for the *flare-sweep* effect, the sweep of the aerodynamic panels were varied on the wingtip, according to Eq. (7). This consisted of warping the wingtip panels into a parallelogram with the same total area.

To account for the change in local AoA, there is a provision within MSC Nastran to specify an initial AoA, camber or twist at each panel via the vector w_j^g[35]. This vector specifies the magnitude of an additional normalised velocity at the collocation point of each aerodynamic panel, acting perpendicular to the panel, which is included in the evaluation of the flow tangency condition at each collocation point. In this paper, this has been utilised to apply a change to the local AoA on the wingtip at a given fold angle, according to the GEM (Eq. (6)). Furthermore, within MSC Nastran an empirical correction factor can be applied, via the W_{kk} matrix, to adjust the lift curve slope of each panel [35]. Due to the large relative thickness of the NACA0015 aerofoil profile used in the experimental model, this correction factor has been utilised to account for the effect of thick aerofoils; with a weighted average of viscous *XFOIL* [38] predictions, across the experimental range of Reynolds numbers, indicating a correction factor of 1.12 should be used for a NACA0015 aerofoil profile, as shown in Fig. 11.

The process for deforming the aerodynamic mesh in the LACA model from the baseline model was automated in a MATLAB [26] routine, allowing new models to be generated and tested rapidly.

B. Static Aeroelastic Response

For a given root AoA and velocity of interest, the static aeroelastic response of the model is calculated using the following algorithm (using an initial coast angle of zero degrees):

1) Generate a LACA model at the given root AoA, velocity, and coast angle
2) Run a static aeroelastic analysis (SOL144) and calculate the coast angle
3) If the coast angle has not converged return to step 1. (a convergence criteria of 0.1 degrees was used throughout this paper)

During step 1 of this process an additional set of corrections are applied to the LACA model to account for the deformation of the inner wing. As is illustrated in Fig. 12 the deformation of the inner wing changes the local dihedral angle at the tip of the inner wing, by an angle Γ_0, which will be further referred to as the Hinge Dihedral Angle (HDA) (as the hinge lies at the tip of the inner wing). As shown in Fig. 12, the HDA alters the direction of the zero-fold-angle of the wingtip. Therefore, the fold angle used to deform the LACA model is the absolute rotation of the wingtip minus the HDA. The deformation of the inner wing can also lead to a change in the local twist angle at the hinge, changing the
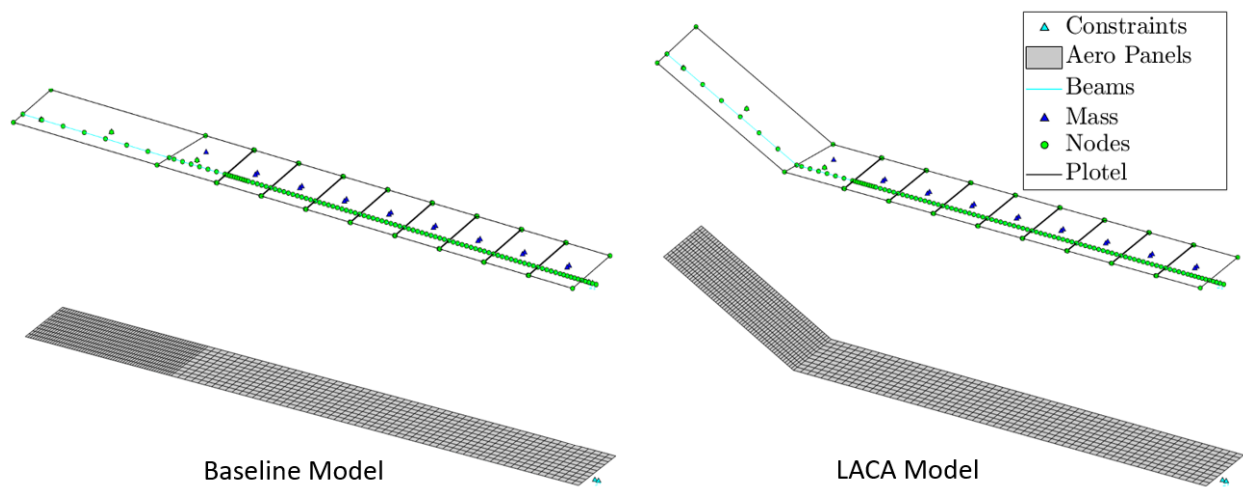

Fig. 10 An example of the LACA structural and aerodynamic mesh, at a fold angle of 30 degrees, compared with the baseline model

local root AoA of the FFWT, this along with the change in HDA are accounted for within the GEM (Eq. (6)).

Additionally, consider the case in which the onset flow velocity is zero, e.g. when the only external forces acting upon the model are gravitational. In this condition the equilibrium position of the wingtip, when there is zero net moment about the hinge, will point vertically down, and there will be a negative HDA, as shown in Fig. 12. Therefore, the fold angle of the wingtip will be less than 90 degrees. However, as only the wingtip is deformed when generating a LACA model, when a model is produced with the correct fold angle, the wingtip will initially not point vertically down, as shown in Fig. 12. Hence, when a gravitational force is applied to this model a proportion of this force will produce a moment about the hinge. As MSC Nastran models gravity as a constant force during the analysis, the magnitude of this moment will not change and the wingtip will not reach the correct equilibrium position. Therefore, a fictitious moment, or *pre-load*, must be applied to the hinge to ensure the moments are balanced about the hinge when the wingtip points vertically down. The magnitude of this *pre-load*, M, can be defined as

$$M = -\sum_{i=1}^{N} m_i g l_i \sin\left(\theta + \Gamma_h\right) \tag{12}$$

where m_n represented the mass of the ith element of the wingtip, and l_i the moment arm of the ith element with respect to the hinge line. During step 1 of the static aeroelastic algorithm, this *pre-load* is automatically calculated and applied to the model as an additional moment about the hinge.

Furthermore, the accurate prediction of drag forces acting on an FFWT may be important when considering the static aeroelastic response of the system, as dependent on the fold angle and attitude of the model, the drag force may have a component which acts as a moment about the hinge.

As the purpose of this paper was not to accurately predict the drag acting on an FFWT, a methodology has instead been developed to gauge the sensitivity of the system to such forces. As such a simple model was developed in which the induced drag on each panel was estimated using the local lift (L_i) and downwash (w_i), such that

$$D_i = L_i \sin(w_i) \tag{13}$$

Then, at each iteration of step 1, the drag on each panel of the wingtip was estimated from the previous run, and the total contribution of these forces to a moment about the hinge axis was calculated. This moment was then used to augment the *pre-load* applied about the hinge of the model in the next iteration.

C. Dynamic Aeroelastic Response

Flutter is a dynamic linear aeroelastic instability that occurs when one of the natural modes of an aircraft becomes unstable. It is characterised by the growth of oscillations with ever increasing amplitude. The accurate prediction of
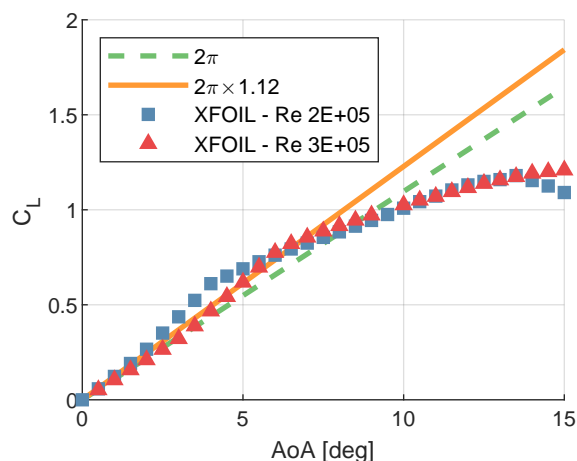

Fig. 11 The variation in the coefficient of lift with AoA for a NACA0015 airfoil using viscous *XFOIL* simulations
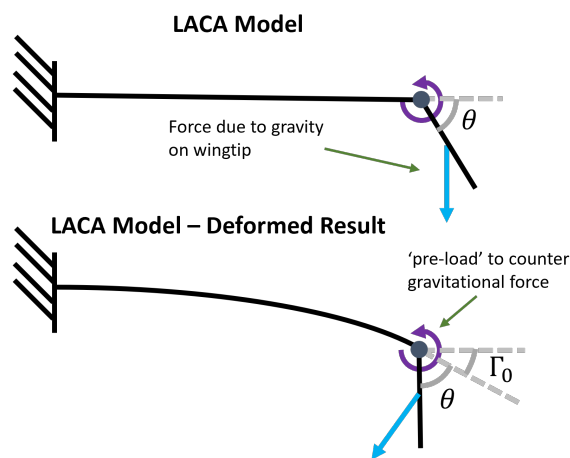

Fig. 12 An illustration of the LACA model at a velocity of zero $m\,s^{-1}$, pre and post applying the SOL144 deformation

the flutter boundary of an aircraft is of prime importance, as the occurrence of such a phenomenon within the flight envelope would be catastrophic. The inbuilt dynamic linear aeroelastic module (SOL145) within MSC Nastran, uses an implementation of the p-k method [23] to predict the variation in the modal frequencies and dampings across a range of flight velocities. These tools are inherently linear, but by applying this linear dynamic analysis about a nonlinear static equilibrium position, a good prediction of the local stability of the system can be achieved [39].

Typically the SOL145 module would be called once across a range of flight velocities. However, as the underlying LACA model will vary with velocity (due to the change in coast angle), the routine is called separately at each velocity using the converged static aeroelastic model predicted using the methodology in section V.B.

Similarly to section V.B, MSC Nastran does not account for the variation in gravitational forces with linear deformations. Once again consider the case illustrated in Fig. 12, of the model at a velocity of zero. In this configuration, dynamic analysis should discover a 'pendulum' mode of the wingtip (in which the wingtip swings like a pendulum), however SOL103 (used for modal analysis with no aerodynamic force) finds no such mode, as MSC Nastran models gravitational forces as a constant that does not change with the deformation of the model. To resolve this effect, an additional stiffness term K_g must be applied to the hinge, which is defined by linearising Eq. (12) about the coast angle θ_c, such that

$$K_g = -\frac{dM}{d\theta}\bigg|_{\theta=\theta_c} = \sum_{i=1}^{N} \left(m_i g l_i \cos\left(\theta_c + \Gamma_h\right)\Gamma_h\right) \tag{14}$$

This hinge stiffness is at a maximum when the wingtip points vertically down and zero at a fold angle of zero degrees. Additionally at positive fold angles (when the wingtip is pointing up) this terms contributes a negative stiffness, destabilising the system.

VI. Results

A. Static Aeroelastic Analysis

Figure 13 shows a comparison between the observed experimental and numerical coast angles. There is good qualitative agreement between the data sets, with the coast angle increasing with velocity - which in turn reduces the local AoA of the wingtip – with the rate of this increase reducing with velocity.

There are however notable offsets between the LACA model and the experimental results, particularly at higher AoAs. At an AoA of 10 degrees, the LACA model consistently over predicts the coast angle by around 15 degrees,
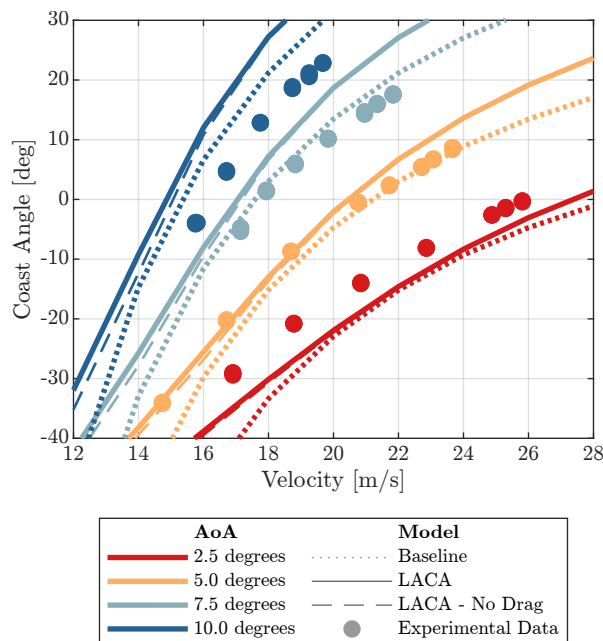

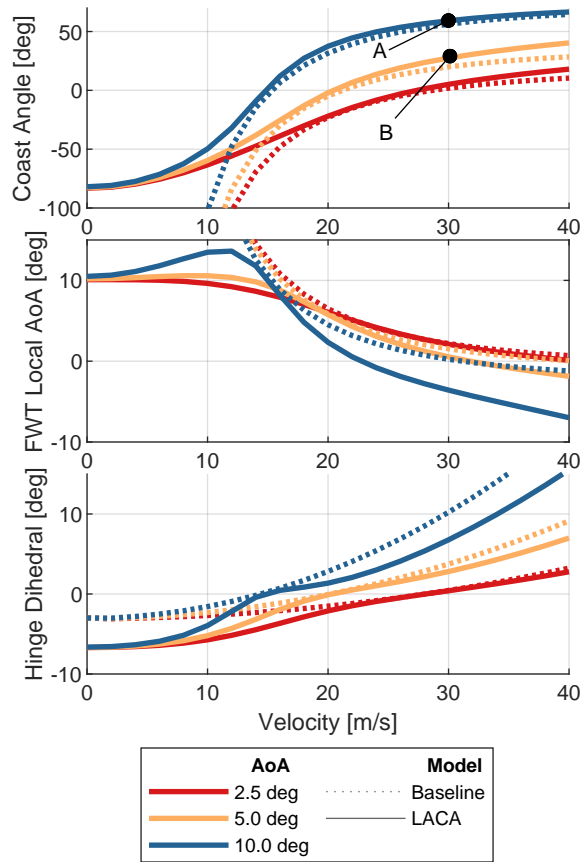**Fig. 13 Experimental and numerical variations in the coast angle with velocity and AoA**

Fig. 14 **The numerical variation in the coast angle, local geometric AoA of the FFWT and the local hinge dihedral angle, with velocity**

suggesting the wingtip of the LACA model generates more lift than the experimental model - as a larger positive coast angle indicates that a smaller or more negative local AoA is required to reduce the aerodynamic loads and balance the moments about the hinge. This overproduction of lift at higher AoAs is not unexpected; as shown in Fig. 11, the constant lift-curve slope used in the numerical modelling over predicts the lift coefficient at an AoA of both 7.5 and 10 degrees. This oversimplification coupled with other nonlinear aerodynamic effects, such as the modelling of flow around the hinge (in reality the hinge line is not parallel to the flow, potentially triggering additional 3D aerodynamic effects such as flow separation) makes the accurate prediction of coast angles particularly difficult within MSC Nastran.

This conclusion is both important and unsurprising. Tools such as MSC Nastran are typically utilised early in the design phase of an aircraft, with there low-fidelity models enabling the dynamic behaviour of an aircraft to be quickly predicted, optimised and varied. This process is built on the assumption that small variations in the deformation do not significantly affect the dynamic behaviour of an aircraft. If however small variations in the coast angle do significantly effect the dynamic behaviour, a different methodology may need to be utilised for configurations incorperating FFWTs.

Quantitative variations aside, the numerical results can be expanded to provide a better understanding of the static response of the system, with Fig. 6 showing the variation in the coast angle, local geometric AoA of the FFWT, and the local dihedral angle at the hinge (the tip of the inner wing) from zero to 40 ms^{-1}. Firstly, as the velocity tends to zero, the static equilibrium position of an FFWT with zero hinge stiffness is completely dominated by gravitational forces. As such, the wingtip acts as a pendulum with a stable equilibrium position pointing vertically down. This effect is shown in Fig. 14, where at zero velocity the LACA model predicts a coast angle just under -90 degrees, due to the deformation of the inner wing changing the HDA (the local dihedral angle at the hinge or tip of the inner wing), reducing the fold angle required for the wingtip to point vertically down. This result is in contrast to that of the baseline model, which tends to a coast angle (or more appropriately a local AoA) of infinity as velocity tends to zero.

Additionally, at zero velocity the weight of the wingtip is transmitted as a shear force through the hinge 'pulling' the

14

inner wing down. As velocity increases the magnitude of the aerodynamic forces acting on the wingtip increase. This produces a positive shear force, reducing the total shear force transmitted across the hinge. This initial unloading of the inner wing quickly reduces the HDA, corresponding to the rapid change between 0 and 15 ms^{-1} in Fig. 14. Beyond this the HDA, is dominated by the loading of the inboard wing, and increases with increasing velocity.

Another interesting feature of Fig. 14 is that the local geometric AoA of the FWT initially increases with velocity, before then reducing. This behaviour is due to the relationship between the fold angle and the local AoA, as described in Eqn. (6), with Fig. 6 showing that the peak AoA for an FFWT with a flare angle of 10 degrees and an AoA of 10 degrees, occurs at a fold angle of roughly -45 degrees, which is the approximate location of the peak in Fig. 14.

As the velocity increases from zero in Fig. 14, the variation between the baseline and LACA model reduces until there is good agreement between the two at low fold angles. As the velocity is increased further, the local AoA of the FFWT reduces to maintain a similar total lift on the wingtip, balancing the aerodynamic and gravitational moments about the hinge. This reduction of the local AoA with velocity ensures that the contribution of wingtip induced drag to the moment about the hinge is minimal at higher velocities, as shown in Fig. 13. Hence, induced drag does not significantly effect the predicted coast angles in flight conditions associated with cruise.

As the velocity tends to infinity - ignoring structural failures or instabilities - the coast angle will tend to the *zero-lift-angle*, e.g. the coast angle at which the local effective AoA on the wingtip is zero - as an infinitesimal AoA is required to balance the gravitational moment. However, as seen in Fig. 14 the geometric AoA of the wingtip tends to a negative value in all test cases.

To explain this behaviour, a modified version of the WT model will be used; imagine a wing with a flare angle of zero degrees at an AoA of zero degrees. By ignoring structural deformations, in this configuration the local AoA of the wingtip will always be zero, regardless of the fold angle. By varying the camber or twist of the inner wing (which is analogous to increasing the root AoA), Fig. 15 shows the effect of the inner wing's spanwise pressure distribution on that of the wingtip. It is important to note here, that although the model is a semispan wing, there is a gap between the root of the wing and the tunnel wall, leading to the reduction of the pressure coefficient towards the root.

Although the local geometric AoA of the wingtip is always zero, Fig. 15 shows that the influence of the inner wing leads to an induced downwash on the wingtip, generating a positive lift. The area under the curve in Fig. 15 is proportional to the total lift acting on the wingtip, with the total lift being shown to increase with both fold angle and root AoA. If the moment about the hinge due to this aerodynamic force is greater then the that due to gravity, a negative local geometric AoA is therefore required to balance the moments about the hinge. Furthermore, as the fold angle increases from zero to 90 degrees, the moment due to gravity about the hinge will decrease (due to the effective shortening of the moment arm). Therefore, at higher fold angles, less aerodynamic force is required to balance the moments about the hinge, requiring a more negative geometric AoA on the wingtip.

The effect of this on a more representative example can be seen in Fig. 16, which shows the spanwise pressure distribution for both the baseline and LACA model at points *A* and *B* in Fig. 14. Figure 16 shows that at the higher root AoA of 10 degrees, the spanwise pressure distribution of the LACA model reduces faster across the wingtip than all the other cases, due to the negative geometric AoA present on the wingtip. Furthermore, as the predicted coast angle
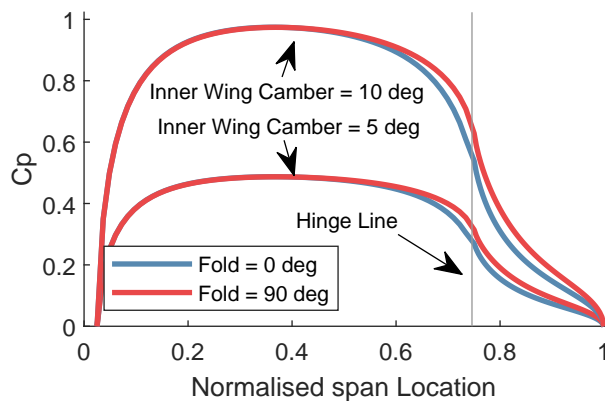

Fig. 15 The spanwise pressure distribution on a wing at a AoA of zero, with the hinge locked at the prescribed fold angle, at a velocity of 30 ms^{-1}
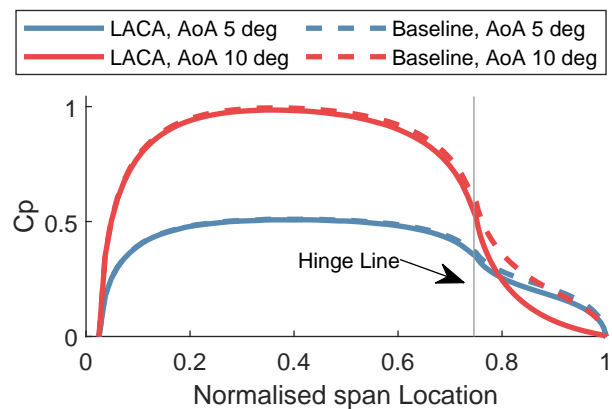

Fig. 16 The spanwise pressure distribution on the LACA model at points A and B in Fig. 14

15

at point *A* is approximately 59 degrees, there is a significant reduction in the gravitational moment about the hinge, meaning a smaller total aerodynamic force is required to balance the moments. This nonlinear effect has been captured in the LACA model, with a significant reduction seen in the total area under the curve on the wingtip in Fig. 16. Where as, the baseline model is still balancing the moment about a fold angle of zero degrees, which requires significantly more lift, and hence has a significant effect on the spanwise pressure distribution. At point *B* the coast angle is much smaller (27 degrees), therefore there is a much smaller variation in the gravitational moment and hence a less pronounced effect on the spanwise pressure distribution.

These observations lead one to conclude that in situations where fold angles are larger than 45 degrees, such as at high AoAs or during manoeuvres, accurately modelling the nonlinear variation in the moment due to gravity with fold angle is important to predict both the coast angle of the wingtip and the pressure distribution along the entire wing.

As a final point in this section, it seems prudent to acknowledge the shape of the pressure distribution in Fig. 16, which deviates from the elliptical or bell shaped distributions which classically provide an optimal lift to drag ratio. As only shear forces are transmitted across the hinge, the lift generated on an FFWT is only enough to support its own weight, where as on a typical configuration this portion of the wing would produce lift far in excess of its own weight. This is why industrial applications of this technology aim to "lock" the wingtip in place during cruise - for optimal aerodynamic efficiency - whilst releasing it during gust encounters and manoeuvres, enhancing the flight envelope of the aircraft, the so called Semi-Aeroelastic Hinge [16, 18].

B. Dynamic Aeroelastic Analysis

At each simulated nonlinear equilibrium position in Fig. 14 linear modal analysis was conducted to track how the modal frequencies and dampings of the model varied with both velocity and root AoA. Figure 17 shows the variation in the first 3 modal frequencies and dampings for both the baseline case and the LACA model at an AoA of 2.5 and
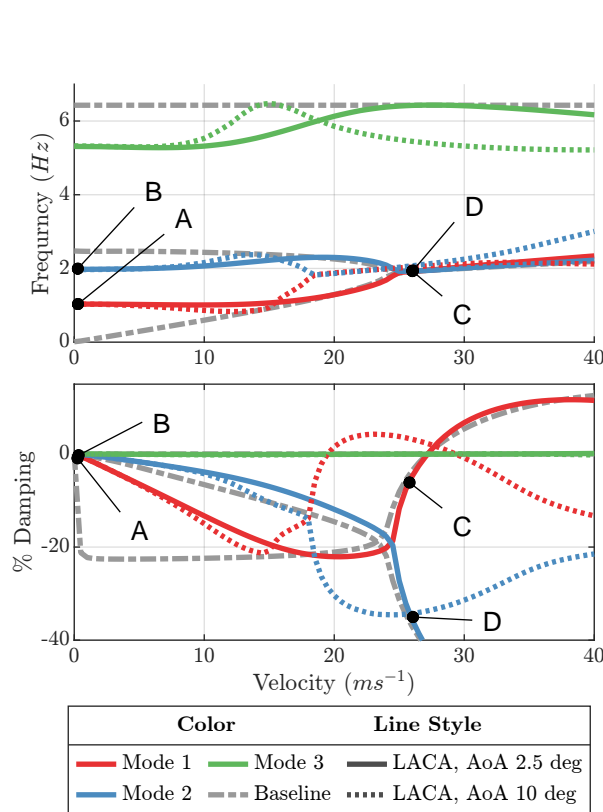

Fig. 17   Variation of the first 3 modal frequencies and dampings, with velocity, of the numerical models at an AoA of 2.5 and 10 degrees
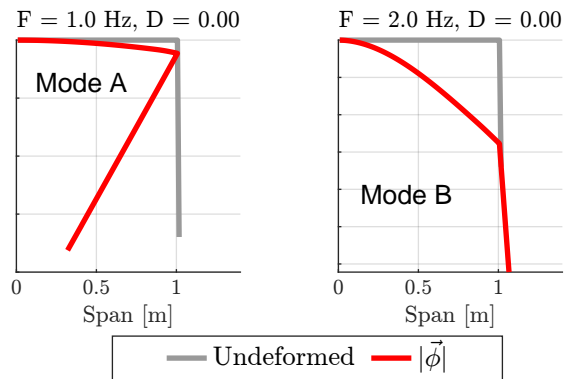

Fig. 18   The corresponding Mode shapes for points A & B in Fig. 17
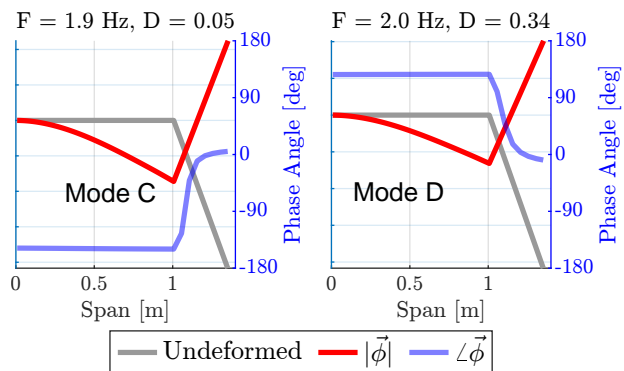

Fig. 19   The corresponding Mode shapes for points C & D in Fig. 17

10 degrees. It should be noted that throughout this paper damping values are represented as the required additional structural damping, g, to give zero overall damping. This is the standard notation, and has its roots in the formulation of the "k"-method for flutter prediction [23]. Consequently, stable damping values are presented as negative, and unstable values as positive.

Regarding Fig. 17, the dynamics of the model - particularly in relation to the primary flutter mechanism – are dominated by the first two modes, and there is good frequency separation between the second and third mode. Therefore, only the first two modes will be studied for the rest of this analysis.

Considering only the baseline case and starting at a velocity of zero, the frequency of the first mode grows linearly - from zero - with velocity, until it interacts with the second mode, leading to flutter. This description is characteristic of linear analysis of a wing incorporating an FFWT, and similar figures have been shown in previous papers [11], with the linear growth in frequency due to the increased aerodynamic stiffness of the wingtip with velocity.

However in reality, at a velocity of zero an FFWT will act as a pendulum with a frequency proportional to the square root of the distance between the hinge and the centre of mass of the wingtip. This effect is captured with the LACA model, with Fig. 17 showing that below a velocity of 5 m/s the first mode it dominated by the effects of gravitational stiffness. This behaviour is further clarified in Fig. 18 which shows that the mode shape at point A in Fig. 17 is dominated by a 'pendulum' motion, oscillating about a equilibrium position pointing vertically down. This mode will be further referred to as the FFWT mode, and the second mode (mode B in Figs. 17 & 18) will be referred to as the first bending mode.

As the velocity is increased from zero, multiple effects are contributing to the changes in both frequency and damping of the first two modes. Firstly, as shown in Fig. 14, the equilibrium position of the wing is changing (most notably the coast angle is increasing), this both reduces the gravitational stiffness of the wingtip and changes its aerodynamic stiffness, as indicated in Fig. 6. Additionally the magnitude of the aerodynamic stiffness is also increasing due to the increasing dynamic pressure. This combination of nonlinear effects leads to highly complex behaviours between a velocity of zero and the linear flutter speed, which are also dependent on the attitude of the model. For example, in Fig. 17, at an AoA of 10 degrees, the frequency of the FFWT mode initially reduces with velocity (due to the rapid change in fold angle reducing the gravitational stiffness), before then rapidly increasing. Whereas in the 2.5 degrees AoA case, there is a gradual increase in frequency with velocity.

The primary flutter mechanism of this system is due to the increasing frequency of the FFWT mode with velocity leading to the coalescence of the first two modes. Most notably, in Fig. 17 the linear flutter speed of the LACA model at an AoA of 10 degrees is significantly less than both the baseline model and the LACA model at an AoA of 2.5 degrees. This finding is due to a rapid increase in the frequency of the FFWT mode between a velocity of approximately 15 to 18 m/s, leading to an earlier coalescence of the first two modes.

Between a velocity of 15 and 18 ms^{-1} Fig. 13 shows that the coast angle of the LACA model at an AoA of 10 degrees increases from 0 to 30 degrees. As shown in Fig. 6, this corresponds to an increase in the magnitude of the aerodynamic stiffness acting upon the wingtip, leading to the increase in frequency of the FFWT mode.

In short, the primary flutter mechanism of this model is the coalescence of the FFWT and first bending mode. At higher velocities the frequency of the FFWT mode is dominated by changes in the aerodynamic stiffness of the wingtip, and at higher AoAs the peak achievable aerodynamic stiffness increases (as shown in Fig. 6). Therefore, the frequency of the FFWT mode can increase at a faster rate with velocity at higher AoAs, causing an earlier coalescence of the first two modes and a significant reduction in the flutter speed.

This conclusion is further supported by the experimental data, with Figs. 20 & 21 showing a comparison between the experimental and numerical modal frequencies and dampings across a range of AoAs. In general there is good correlation between the data sets, particularly in the frequencies at lower AoAs, with both methods of excitation producing comparable results.

One exception is the measured frequencies of the FFWT mode at an AoA at 7.5 and 10 degrees, in which the experimental frequencies are less than that predicted by the LACA model. This is likely due to two factors. Firstly, at higher AoAs stall and 3D aerodynamic effects may significantly change the aerodynamic stiffness of the wingtip. Secondly, there is an over prediction of the coast angle in these conditions (as shown in Fig. 13), with the lower coast angles seen experimentally resulting in a lower aerodynamic stiffness of the FFWT, reducing the measured frequency.

Equally, when considering results close to the linear flutter speed. In the simulated results the two modes coalesce in frequency but diverge in damping. This behaviour is not however clear in the experimental results, with only the 2.5 degrees root AoA case showing such a trend in Fig. 20. By looking back at Fig. 17 we can inspect the modes shapes at points C & D, shown in Fig. 19. Due to the influence of damping, these modes shapes are complex, with the magnitude at each node representing the amplitude of oscillation and the argument the phase shift of the oscillation. Figure 19

17

shows that the mode shape at points C and D are similar, and only differ by the phase angle of the wingtip. These similar mode shapes, coupled with the poor frequency separation and noise in the experimental data, meant it was very difficult to separate these modes. Therefore, the disparities seen in the experimental damping trends towards the linear flutter speed are likely an artifact of the ERA rather than a difference between the experimental and numerical models.

A comparison of the flutter speeds in Figs. 20 & 21 can be seen in Fig. 22 . The experimental flutter speeds were estimated by incrementally increasing the speed in the step response test until exponential growth of an oscillatory motion was observed (at which point the string attached to the model was pulled taut to stop the motion). Therefore, the experimental flutter speeds presented in Fig. 22 represent the range between the highest stable speed and the first speed at which the model was unstable. Compared with the baseline model, by simply varying the root AoA a maximum reduction of 28% was seen in the flutter speed of the experimental model. This variation is due the change in the aerodynamic stiffness of the wingtip at different coast angles, which for low fold angles is primarily driven by the *fold-AoA* effect described in section III. As such it is envisaged that the scale of this effect will reduce with increasing flare angle, due to the increased dominance of the *flare-twist* effect. This can be visually seen in Fig. 6 in which the variation of the peak aerodynamic stiffness of the wingtip decreases with flare angle. It is worth highlighting again that the peak aerodynamic stiffness in Fig. 6 occurs at non-zero AoAs and coast angles, therefore, when geometric nonlineariteis are accounted for, the worst-case predicted flutter speed will always be lower than that predicted by the linear model.

Figure 22 also indicates a good correlation between the LACA and experimental values, particularly at high fold angles further supporting the conclusion that increasing the root AoA, increases the aerodynamic stiffness of the FFWT mode and therefore reduces the flutter speed of the model. However, there is a larger error between the flutter speeds of the LACA and experimental models at lower AoAs.

The sensitivity of the LACA model to variations in the coast angle also decrease with increasing AoA (the error bars of the LACA model in Fig. 22 represent the flutter speeds at ±5 degrees coast angle). This greater sensitivity emerges
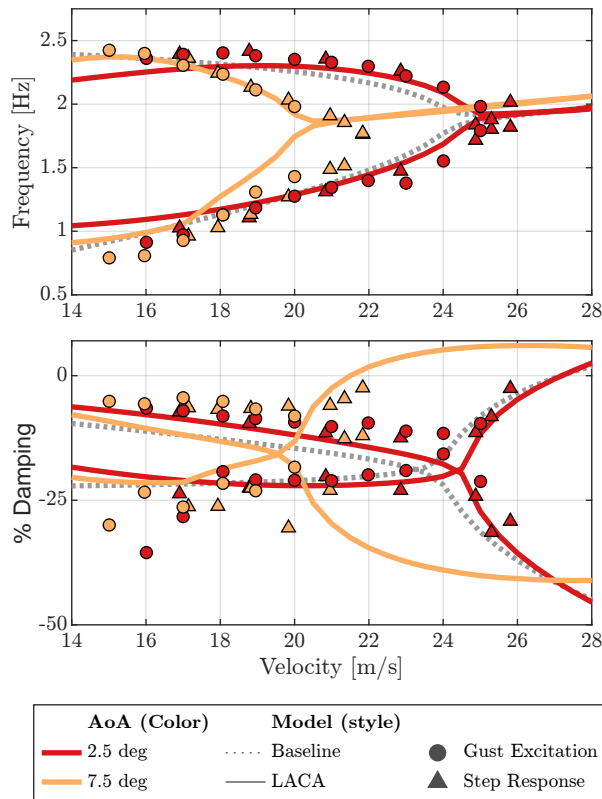

Fig. 20 Variation in modal frequencies and damping, with velocity, of the numerical and experimental models, at an AoA of 2.5 and 7.5 degrees
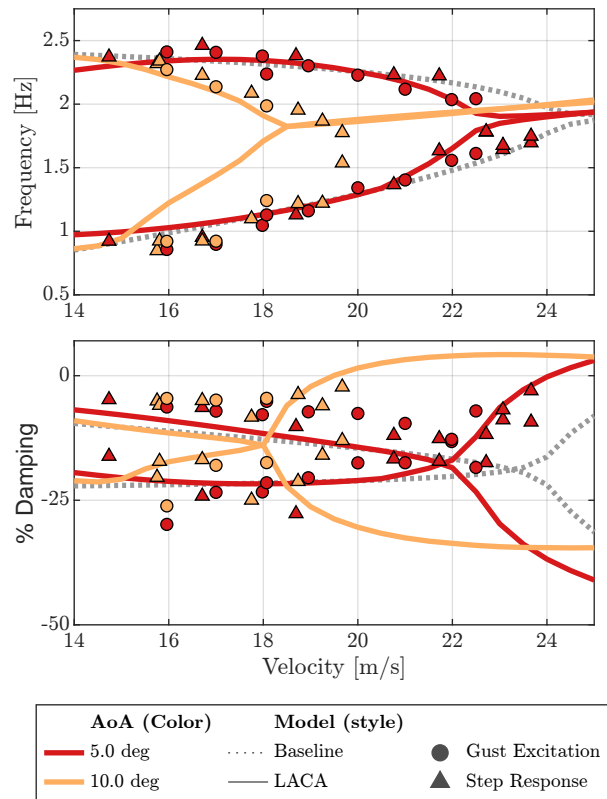
Fig. 21 Variation in modal frequencies and damping, with velocity, of the numerical and experimental models, at an AoA of 5 and 10 degrees
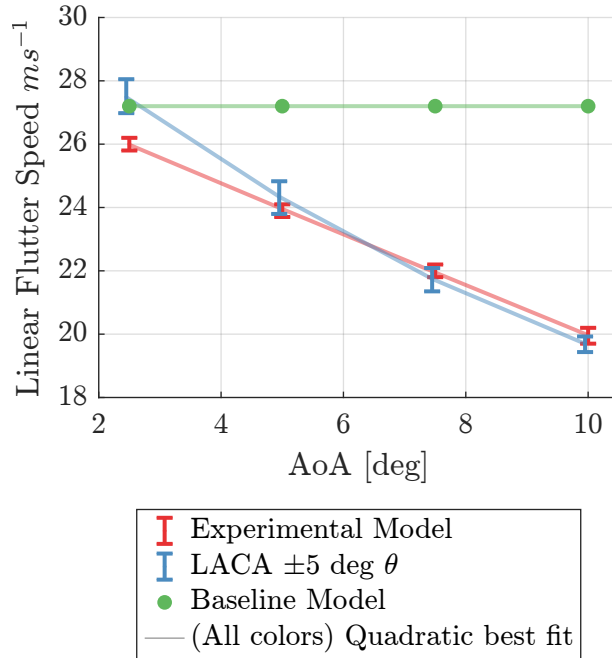
Fig. 22 The numerical and experimental predicted flutter speeds

from the variation in rate of change of aerodynamic stiffness with coast angle, as shown in Fig. 6. Considering again the difficulties highlighted in section VI.A in regards accurately predicting the coast angle in medium to low fidelity model, Fig. 22 highlights that relatively small uncertainties in the predicted coast angle can have a noticeable impact on the flutter speed, with a ~ 3.5% variation in the flutter speed seen by varying the coast angle by ±5 degrees at an AoA of 5 degrees. This suggests a different approach may be required for the estimation of the flutter boundary in the early design stage of systems incorporating FFWTs. For example, instead of predicting the stability of an aircraft about the coast angle, one could instead calculate the stability of the aircraft about the worst-case coast angle in each flight condition.

VII. Conclusions

The majority of research into FFWTs has been conducted in the linear regime, linearised about a fold angle of zero degrees. However, large rotations of the wingtip have been shown in nearly all studies, including wind tunnel experiments and flight tests of a small Unmanned Aerial Vehicle (UAV). Such large rotations are analogous to those seen in the modelling of highly flexible wings, and can introduce geometric and aerodynamic nonlinearities that significantly affect the overall system dynamics. This paper explored how large variations in the fold angle of a wing incorporating Flared Folding Wingtips (FFWT) could impact its static and dynamic behaviour and, in particular, reduce the predicted linear flutter speed when compared to linear methods. To do this, a geometrically exact expression was formulated to describe the change in both the local AoA and sideslip angle on a wingtip, across all fold angles. This expression highlighted three primary mechanisms driving the geometric nonlinearities of FFWT devices. Additionally, this expression indicated that the aerodynamic stiffness of an FFWT is a function of the fold angle, therefore, changes to the attitude of the model (which can alter the coast angle of a wingtip) can affect quantities such as the linear flutter speed. This effect was then verified using both: a wind tunnel model of a flexible semi-span wing incorporating an FFWT, and a new numerical modelling technique, utilising MSC Nastran, which linearised a model about the equilibrium position of the wingtip. The results of these experiments showed that the geometric nonlinearities introduced due to the large deformations of FFWTs can significantly affect the dynamics of the system, with flutter speeds varying by over 25%, simply by changing the root angle of attack of the model. Furthermore, good agreement was found between the experimental and numerical results.

Acknowledgments

References

[1] Fichert, F., Forsyth, P., and Niemeier, H.-M., *Aviation and Climate Change: Economic Perspectives on Greenhouse Gas Reduction Policies*, 1st ed., Routledge, London, 2020. https://doi.org/10.4324/9781315572406.

[2] Calderon, D., Cooper, J., Lowenberg, M., Neild, S., and Coetzee, E., "Sizing High-Aspect-Ratio Wings with a Geometrically Nonlinear Beam Model," *Journal of Aircraft*, Vol. 56, No. 4, 2019, pp. 1455–1470. https://doi.org/10.2514/1.C035296.

[3] Anon., "Icao's Policies on Charges for Airports and Air Navigation Services," Tech. Rep. 9082, International Civil Aviation Organization, 2009. URL https://www.icao.int/publications/Documents/9082_8ed_en.pdf.

[4] Bradley, M. K., Droney, C. K., and Allen, T. J., "Subsonic Ultra Green Aircraft Research. Phase Ii-Volume I; Truss Braced Wing Design Exploration,," Tech. Rep. CR-2015-218704, NASA, 2015. URL https://ntrs.nasa.gov/citations/20150017036.

[5] Anon, *Annex 14*, 8th ed., Aerodromes, Vol. 1, International Civil Aviation Orginization, Montréal, Quebec, 2018.

[6] Barnes, C. H., *Shorts Aircraft since 1900*, Putnam; Aero Publishers, London; Fallbrook (Calif.), 1967.

[7] Lassen, M., Douglas, C., Jones, K. T., and Kenning, T. B., *Wing Fold Controller*, Office, European Patent, 2018. EP2727829B1.

[8] Khodaparast, H. H., and Cooper, J. E., "Rapid Prediction of Worst-Case Gust Loads Following Structural Modification," *AIAA Journal*, Vol. 52, No. 2, 2014, pp. 242–254. https://doi.org/10.2514/1.J052031.

[9] Castrichini, A., Hodigere Siddaramaiah, V., Calderon, D. E., Cooper, J. E., Wilson, T., and Lemmens, Y., "Nonlinear Folding Wing Tips for Gust Loads Alleviation," *Journal of Aircraft*, Vol. 53, No. 5, 2016, pp. 1391–1399. https://doi.org/10.2514/1.c033474.

[10] Cheung, R. C. M., Rezgui, D., Cooper, J. E., and Wilson, T., "Testing of a Hinged Wingtip Device for Gust Loads Alleviation," *Journal of Aircraft*, Vol. 55, No. 5, 2018, pp. 2050–2067. https://doi.org/10.2514/1.c034811.

[11] Castrichini, A., Siddaramaiah, V. H., Calderon, D. E., Cooper, J. E., Wilson, T., and Lemmens, Y., "Preliminary Investigation of Use of Flexible Folding Wing Tips for Static and Dynamic Load Alleviation," *The Aeronautical Journal*, Vol. 121, No. 1235, 2017, pp. 73–94. https://doi.org/10.1017/aer.2016.108.

[12] Dussart, G., Yusuf, S., and Lone, M., "Identification of in-Flight Wingtip Folding Effects on the Roll Characteristics of a Flexible Aircraft," *Aerospace*, Vol. 6, No. 6, 2019, p. 63. https://doi.org/10.3390/aerospace6060063.

[13] Wilson, T., Castrichini, A., Azabal, A., Cooper, J., Ajaj, R., and Herring, M., "Aeroelastic Behaviour of Hinged Wing Tips," International Forum of Aeroelasticity and Structural Dynamics, 2017. URL www.asdjournal.org/public/Proceedings/IFASD_2017/IFASD-2017-216.pdf.

[14] Castrichini, A., Wilson, T., Saltari, F., Mastroddi, F., Viceconti, N., and Cooper, J., "Aeroelastics Flight Dynamics Coupling Effects of the Semi-Aeroelastic Hinge Device," *Journal of Aircraft*, 2019, pp. 1–9. https://doi.org/10.2514/1.C035602.

[15] Cheung, R. C. M., Rezgui, D., Cooper, J. E., and Wilson, T., "Testing of Folding Wingtip for Gust Load Alleviation of Flexible High-Aspect-Ratio Wing," *Journal of Aircraft*, 2020, pp. 1–13. https://doi.org/10.2514/1.c035732.

[16] Gu, H., Healy, F., and Cooper, J. E., "Sizing of High Aspect Ratio Wings Incorporating Folding Wingtip," AeroBest, Lisbon, Portugal, 2021.

[17] Balatti, D., Haddad Khodaparast, H., Friswell, M. I., Manolesos, M., and Amoozgar, M., "The Effect of Folding Wingtips on the Worst-Case Gust Loads of a Simplified Aircraft Model," *Proceedings of the Institution of Mechanical Engineers, Part G: Journal of Aerospace Engineering*, 2021. https://doi.org/10.1177/09544100211010915.

[18] Wilson, T., Kirk, J., Hobday, J., and Castrichini, A., "Small Scale Flying Demonstration of Semi Aeroelastic Hinged Wing Tips," International Forum on Aeroelasticity and Structural Dynamics, Savannah, Georgia, USA, 2019. URL www.asdjournal.org/public/Proceedings/IFASD_2019/IFASD-2019-076.pdf.

[19] Healy, F., Cheung, R., Neofet, T., Lowenberg, M., Rezgui, D., Cooper, J., Castrichini, A., and Wilson, T., "Folding Wingtips for Improved Roll Performance," *Journal of Aircraft*, 2021, pp. 1–14. https://doi.org/10.2514/1.C036372.

[20] Howcroft, C., Calderon, D., Lambert, L., Castellani, M., Cooper, J. E., Lowenberg, M. H., and Neild, S., "Aeroelastic Modelling of Highly Flexible Wings," 15th Dynamics Specialists Conference, San Diego, California, USA, 2016. https: //doi.org/10.2514/6.2016-1798.

[21] Wilson, T., Castrichini, A., Paterson, J., and Arribas Ardura, R., "Non-Linear Aeroelastic Behaviour of Hinged Wing Tips," 6th Aircraft Structural Design Conference, We The Curious, Bristol, UK, 2018. https://doi.org/10.2514/6.2017-0502.

[22] Conti, C., Saltari, F., Mastroddi, F., Wilson, T., and Castrichini, A., "Quasi-Steady Aeroelastic Analysis of the Semi-Aeroelastic Hinge Including Geometric Nonlinearities," *Journal of Aircraft*, 2021, pp. 1–11. https://doi.org/10.2514/1.C036115.

[23] Wright, J., and Cooper, J. E., *Introduction to Aircraft Aeroelasticity and Loads*, Aerospace Series, Wiley, Chichester UK, 2015. https://doi.org/10.1002/9781118700440.

[24] *Msc Nastran*, Software Package, Ver. 2018.1, MSC Software GmbH, Munich, Germany, 2018.

[25] Jones, R. T., and Cohen, D., *Fundamental Considerations in the Development of Wings for High Speeds*, Princeton University Press, 1960, pp. 3–48. URL http://www.jstor.org/stable/j.ctt183pq8s.4.

[26] *Matlab R2020b*, Software Package, Ver. 9.9.0.1592791, The MathWorks Inc., Natick, Massachusetts, 2020.

[27] Wood, K., Cheung, R., Richardson, T., Cooper, J., Darbyshire, O., and Warsop, C., "A New Gust Generator for a Low Speed Wind Tunnel: Design and Commissioning," 55th AIAA Aerospace Sciences Meeting, Grapevine, Texas, 2017. https://doi.org/10.2514/6.2017-0502.

[28] Anon., "Certification Specifications and Acceptable Means of Compliance for Large Aeroplanes Cs-25 Amendment 26," Tech. rep., Easa, 2020.

[29] Fu, Z.-F., and He, J., *Modal Analysis*, Butterworth-Heinemann, Jordan Hill, Oxford, UK, 2001, chap. Experimental Modal Analysis - Time Domain. https://doi.org/10.1016/B978-0-7506-5079-3.X5000-1.

[30] Juang, J.-N., and Pappa, R. S., "An Eigensystem Realization Algorithm for Modal Parameter Identification and Model Reduction," *Journal of Guidance, Control, and Dynamics*, Vol. 8, No. 5, 1985, pp. 620–627. https://doi.org/10.2514/3.20031.

[31] Farrar, C. R., and James III, G. H., "System Identification from Ambient Vibration Measurements on a Bridge," *Journal of Sound and Vibration*, Vol. 205, No. 1, 1997, pp. 1–18. https://doi.org/10.1006/jsvi.1997.0977.

[32] Albano, E., and Rodden, W. P., "A Doublet-Lattice Method for Calculating Lift Distributions on Oscillating Surfaces in Subsonic Flows," *AIAA Journal*, Vol. 7, No. 2, 1969, pp. 279–285. https://doi.org/10.2514/3.5086.

[33] Kalman, T. P., Rodden, W. P., and Giesing, J. P., "Application of the Doublet-Lattice Method to Nonplanar Configurations in Subsonic Flow," *Journal of Aircraft*, Vol. 8, No. 6, 1971, pp. 406–413. https://doi.org/10.2514/3.59117.

[34] Giesing, J. P., Kalman, T. P., and Rodden, W. P., "Subsonic Steady and Oscillatory Aerodynamics for Multiple Interfering Wings and Bodies," *Journal of Aircraft*, Vol. 9, No. 10, 1972, pp. 693–702. https://doi.org/10.2514/3.59066.

[35] Rodden, W., and Johnson, E., *Msc Nastran Aeroelastic Analysis: User's Guide, Version 68*, MacNeal-Schwendler Corporation, 2014.

[36] Ferguson, S., Viisoreanu, A., Schwimley, S., and Miller, G., "Integrated Nonlinear Aerodynamic-Structural Tool for External Loads Development," AIAA Atmospheric Flight Mechanics Conference and Exhibit, 2007. https://doi.org/10.2514/6.2007-6382.

[37] Scott, R., Bartels, R., and Kandil, O., *An Aeroelastic Analysis of a Thin Flexible Membrane*, Structures, Structural Dynamics, and Materials and Co-Located Conferences, American Institute of Aeronautics and Astronautics, 2007. https://doi.org/10.2514/6.2007-2316, URL https://doi.org/10.2514/6.2007-2316.

[38] Drela, M., "Xfoil: An Analysis and Design System for Low Reynolds Number Airfoils," *Low Reynolds Number Aerodynamics*, edited by T. J. Mueller, Springer Berlin Heidelberg, 1989, pp. 1–12. https://doi.org/10.1007/978-3-642-84010-4_1.

[39] Dimitriadis, G., *Introduction to Nonlinear Aeroelasticity*, 2017, chap. 2, pp. 9–61. https://doi.org/10.1002/9781118756478.ch2.